

# N-HiTS: Neural Hierarchical Interpolation for Time Series Forecasting

Cristian Challu\*<sup>1</sup> Kin G. Olivares\*<sup>1</sup> Boris N. Oreshkin<sup>2</sup> Federico Garza<sup>3</sup> Max Mergenthaler<sup>3</sup>  
Artur Dubrawski<sup>1</sup>

## Abstract

Recent progress in neural forecasting accelerated improvements in performance of large-scale forecasting systems. Yet, long horizon forecasting remains a very difficult task. Two common challenges afflicting the long horizon forecasting are the volatility of the predictions and their computational complexity. In this paper we introduce N-HiTS, a model which addresses both challenges by incorporating novel hierarchical interpolation and multi-rate data sampling techniques. These techniques enable the proposed method to assemble its predictions sequentially, selectively emphasizing components with different frequencies and scales, while decomposing the input signal and synthesizing the forecast. We conduct an extensive empirical evaluation demonstrating the advantages of N-HiTS over the state-of-the-art long-horizon forecasting methods. On an array of multivariate forecasting tasks, the proposed method provides an average accuracy improvement of 25% over the latest Transformer architectures while reducing the computation time by an order of magnitude. Our code is available in this repository.

## 1. Introduction

Long-horizon forecasting is critical in many important applications including risk management and planning. Notable examples include power plant maintenance scheduling (Hyndman & Fan, 2009) and planning for infrastructure construction (Ziel & Steinert, 2018), as well as early warning systems that help mitigate vulnerabilities due to extreme weather events (Basher, 2006; Field et al., 2012). In healthcare, predictive monitoring of vital signs enables detection of preventable adverse outcomes and application of life-saving interventions (Churpek et al., 2016).

\*Equal contribution <sup>1</sup>Auton Lab, School of Computer Science, Carnegie Mellon University <sup>2</sup>Unity Technologies, Labs, Montreal, QC, Canada <sup>3</sup>Nixtla. Correspondence to: Cristian Challu <cchallu@cs.cmu.edu>, Kin G. Olivares <kdgutier@cs.cmu.edu>.

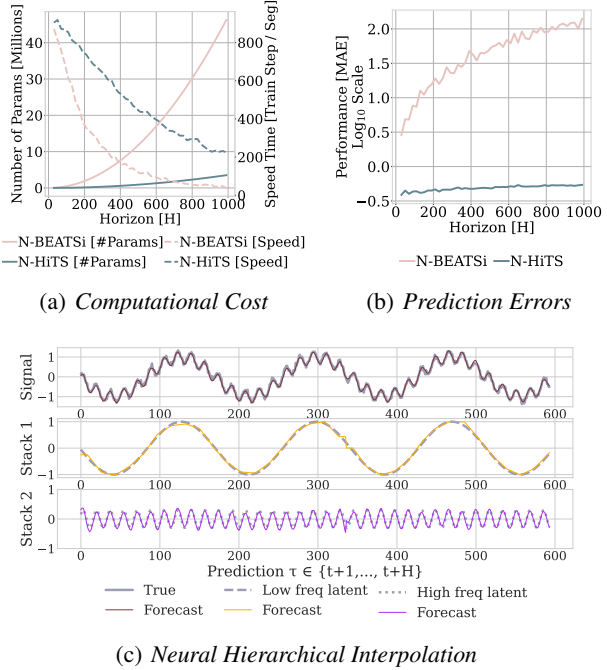


Figure 1. (a) The computational costs in time and memory (b) and *mean absolute errors* (MAE) of the predictions of a high capacity fully connected model exhibit evident deterioration with growing forecast horizons. (c) Specializing a flexible model’s outputs in the different frequencies of the signal through hierarchical interpolation combined with multi-rate input processing offers a solution.

Recently, neural time series forecasting has progressed in a few promising directions. First, the architectural evolution included adoption of the attention mechanism and the rise of Transformer-inspired approaches (Li et al., 2019; Fan et al., 2019; Alaa & van der Schaar, 2019; Lim et al., 2021), as well as introduction of attention-free architectures composed of deep stacks of fully connected layers (Oreshkin et al., 2020; Olivares et al., 2021a). Both of these approaches are relatively easy to scale up in terms of capacity, compared to LSTMs, and have proven to be capable of capturing long-range dependencies. The attention-based approaches are very generic as they can explicitly model direct interactions between every pair of input-output elements. Unsurprisingly, they happen to be the most computationally expensive. The architectures based on fully connected

stacks capture input-output relationships implicitly, however they tend to be more compute-efficient. Second, the recurrent forecast generation strategy has been replaced with the multi-step prediction strategy in both of these approaches. Aside from its convenient bias-variance benefits and robustness (Marcellino et al., 2006; Atiya & Taieb, 2016), the multi-step strategy has enabled the models to efficiently predict long sequences in a single forward pass (Wen et al., 2017; Zhou et al., 2020; Lim et al., 2021).

Despite all the recent progress, long-horizon forecasting remains challenging for neural networks, because their unbounded expressiveness translates directly into *excessive computational complexity* and *forecast volatility*, both of which become especially pronounced in this context. For instance, both attention and fully connected layers scale quadratically in memory and computational cost with respect to the forecasting horizon length. Fig. 1 illustrates how forecasting errors and computation costs inflate dramatically with growing forecasting horizon in the case of the fully connected architecture electricity consumption predictions. Attention-based predictions show similar behavior.

Neural long-horizon forecasting research has mostly limited to the attempts of making self-attention sparse (Child et al., 2019; Li et al., 2019; Zhou et al., 2020), local (Li et al., 2019), and cleverly redefining it through locality-sensitive hashing (Kitaev et al., 2020) or Fourier transformations (Wu et al., 2021). Although that research has led to incremental improvements in compute cost and accuracy, the silver bullet long-horizon forecasting solution is yet to be found. In this paper we make a bold step in this direction by developing a novel forecasting approach that cuts long-horizon compute cost by an order of magnitude while simultaneously offering 25% accuracy improvements on a large array of multi-variate forecasting datasets compared to existing state-of-the-art Transformer-based techniques. We redefine existing fully-connected N-BEATS architecture (Oreshkin et al., 2020) by enhancing its input decomposition via multi-rate data sampling and its output synthesizer via multi-scale interpolation. Our extensive experiments show the importance of the proposed novel architectural components and validate significant improvements in accuracy and computational complexity of the proposed algorithm. Our contributions are summarized below:

- (i) **Multi-Rate Data Sampling:** We incorporate sub-sampling layers in front of fully-connected blocks, significantly reducing the memory footprint and the amount of computation needed, while maintaining the ability to model long-range dependencies.
- (ii) **Hierarchical Interpolation:** We enforce smoothness of the multi-step predictions by reducing the dimensionality of neural network's prediction and matching

its time scale with that of the final output via multi-scale hierarchical interpolation.

- (iii) **N-HiTS architecture:** A novel way of hierarchically synchronizing the rate of input sampling with the scale of output interpolation across blocks, which induces each block to specialize on forecasting its own frequency band of the time-series signal.
- (iv) **State-of-the-art results** on six well-established multi-variate forecasting benchmarks.

The remainder of this paper is structured as follows. Section 2 reviews relevant literature, Section 3 introduces notation and describes the methodology, Sections 4 and 5 describe and analyze our empirical findings. Finally, Section 6 concludes the paper.

## 2. Related Work

**Deep time-series forecasting.** Over the past few years, deep forecasting methods have become ubiquitous in industrial forecasting systems, with examples in optimal resource allocation and planning in transportation (Laptev et al., 2017), large e-commerce retail (Wen et al., 2017; Olivares et al., 2021b), or financial trading (Banushev & Barclay, 2021). The evident success of the methods in recent forecasting competitions (Makridakis et al., 2020; 2021) has renovated the interest within the academic community (Benidis et al., 2020). In the context of multi-variate long-horizon forecasting, Transformer-based approaches have dominated the landscape in the recent years, including Autoformer (Wu et al., 2021), an encoder-decoder model with decomposition capabilities and an approximation to attention based on Fourier transform, Informer (Zhou et al., 2020), Transformer with MLP based multi-step prediction strategy, that approximates self-attention with sparsity, Reformer (Kitaev et al., 2020), Transformer that approximates attention with locality-sensitive hashing and LogTrans (Li et al., 2019), Transformer with local/log-sparse attention.

**Multi-step forecasting.** Investigations of the bias/variance trade-off in multi-step forecasting strategies reveal that the *direct* strategy, which allocates a different model for each step, has low bias and high variance, avoiding error accumulation across steps, exhibited by the classical *recursive* strategy, but losing in terms of net model parsimony. Conversely, in the *joint* forecasting strategy, a single model produces forecasts for all steps in one shot, striking the perfect balance between variance and bias, avoiding error accumulation and leveraging shared model parameters (Bao et al., 2014; Atiya & Taieb, 2016; Wen et al., 2017).

**Multi-rate input sampling.** Previous forecasting literature recognized challenges of extremely long horizon pre-

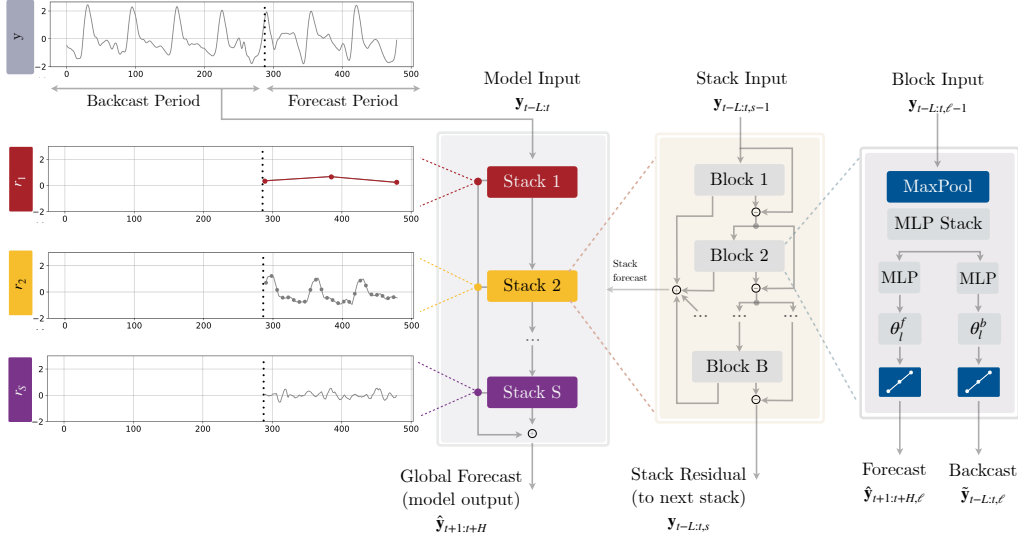


**Figure 2.** N-HiTS architecture. The model is composed of several MLPs with ReLU nonlinearities. Blocks are connected via doubly residual stacking principle with the backcast  $\tilde{y}_{t-L:t,\ell}$  and forecast  $\hat{y}_{t+1:t+H,\ell}$  outputs of the  $\ell$ -th block. Multi-rate input pooling, hierarchical interpolation and backcast residual connections together induce the specialization of the additive predictions in different signal bands, reducing memory footprint and compute time, improving architecture parsimony and accuracy.

dictions, and proposed *mixed data sampling regression* (MIDAS; Ghysels et al. 2007; Armesto et al. 2010) to ameliorate the problem of parameter proliferation while preserving high frequency temporal information. MIDAS regressions maintained the classic *recursive* forecasting strategy of linear auto-regressive models, but defined a parsimonious fashion of feeding the inputs into the model.

**Interpolation.** Interpolation has been extensively used to augment the resolution of modeled signals in many fields such as signal and image processing (Meijering, 2002). In time-series forecasting, its applications range from completing unevenly sampled data and noise filters (Chow & Ioh Lin, 1971; Fernandez, 1981; Shukla & Marlin, 2019; Rubanova et al., 2019) to fine-grained quantile-regressions with recurrent networks (Gasthaus et al., 2019). To our knowledge, temporal interpolation has not been used to induce multi-scale hierarchical time-series forecasts.

### 3. N-HiTS Methodology

In this section, we describe our proposed approach, N-HiTS, whose high-level diagram and main principles of operation are depicted in Fig. 2. Our method extends the *Neural Basis Expansion Analysis* approach (N-BEATS; Oreshkin et al. 2020) in a few important respects, making it more accurate and computationally efficient, especially in the context of long-horizon forecasting. In essence, our approach uses multi-rate sampling of the input signal and multi-scale synthesis of the forecast, resulting in a hierarchical construction of forecast, greatly reducing computational

requirements and improving forecasting accuracy.

N-BEATS performs local nonlinear projections onto basis functions across multiple blocks. Each block consists of a *multilayer perceptron* (MLP), which learns to produce coefficients for the backcast and forecast outputs of its basis. The backcast output is used to clean the inputs of subsequent blocks, while the forecasts are summed to compose the final prediction. The blocks are grouped in stacks, each specialized in learning a different characteristic of the data using a different set of basis functions. The overall network input,  $y_{t-L:t}$ , consists of  $L$  lags of the target time-series  $y$ .

Similar to N-BEATS, N-HiTS is composed of  $S$  stacks,  $B$  blocks each. Each block contains an MLP predicting forward and backward basis coefficients. The next subsections describe the novel components of our architecture. Note that in the following, we skip the stack index  $s$  for brevity.

#### 3.1. Multi-Rate Signal Sampling

At the input to each block  $\ell$ , we propose to use a MaxPool layer with kernel size  $k_\ell$  to help it focus on analyzing components of its input with a specific scale. Larger  $k_\ell$  will tend to cut more high-frequency/small-time-scale components from the input of the MLP, forcing the block to focus on analyzing large scale/low frequency content. We call this *multi-rate signal sampling*, referring to the fact that the MLP in each block faces a different effective input signal sampling rate. Intuitively, this helps the blocks with larger pooling kernel size  $k_\ell$  focus on analyzing large scale components critical for producing consistent long-horizon forecasts.

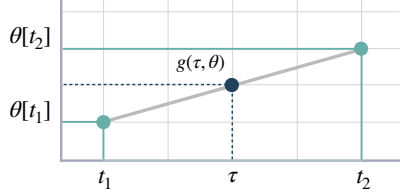


Figure 3. The interpolation enhancement to the multi-step forecasting strategy allows N-HiTS to reduce the volatility of the predictions through smoothness.

Additionally, multi-rate processing reduces the width of the MLP input for most blocks, limiting the memory footprint and the amount of computation as well as reducing the number of learnable parameters and hence alleviating the effects of overfitting, while maintaining the original receptive field. Given block  $\ell$  input  $\mathbf{y}_{t-L:t,\ell}$  (the input to the first block  $\ell = 1$  is the network-wide input,  $\mathbf{y}_{t-L:t,1} \equiv \mathbf{y}_{t-L:t}$ ), this operation can be formalized as follows:

$$\mathbf{y}_{t-L:t,\ell}^{(p)} = \text{MaxPool}(\mathbf{y}_{t-L:t,\ell}, k_\ell) \quad (1)$$

### 3.2. Non-Linear Regression

Following subsampling, block  $\ell$  looks at its input and non-linearly regresses forward  $\theta_\ell^f$  and backward  $\theta_\ell^b$  interpolation coefficients using an MLP that learns hidden vector  $\mathbf{h}_\ell \in \mathbb{R}^{N_h}$ , which is then linearly projected:

$$\begin{aligned} \mathbf{h}_\ell &= \text{MLP}_\ell \left( \mathbf{y}_{t-L:t,\ell}^{(p)} \right), \\ \theta_\ell^f &= \text{LINEAR}^f(\mathbf{h}_\ell), \quad \theta_\ell^b = \text{LINEAR}^b(\mathbf{h}_\ell). \end{aligned} \quad (2)$$

The coefficients are then used to synthesize backcast  $\tilde{\mathbf{y}}_{t-L:t,\ell}$  and forecast  $\hat{\mathbf{y}}_{t+1:t+H,\ell}$  outputs of the block, via the process described below.

### 3.3. Hierarchical Interpolation

In most multi-horizon forecasting models, the cardinality of the neural network prediction equals the dimensionality of horizon,  $H$ . For example, in N-BEATS  $|\theta_\ell^f| = H$ ; in Transformer-based models, decoder attention layer cross-correlates  $H$  output embeddings with  $L$  encoded input embeddings ( $L$  tends to grow with growing  $H$ ). This leads to quick inflation in compute requirements and unnecessary explosion in model expressiveness (and as a result, in overfitting) as horizon  $H$  increases.

To combat these issues, N-HiTS uses *interpolation* along time dimension. It defines the dimensionality of its interpolation coefficients in terms of the *expressiveness ratio*  $r_\ell$  that controls the number of parameters per unit of output time,  $|\theta_\ell^f| = \lceil r_\ell H \rceil$ . To recover the original output sampling rate and predict all  $H$  points in the target horizon, N-HiTS uses

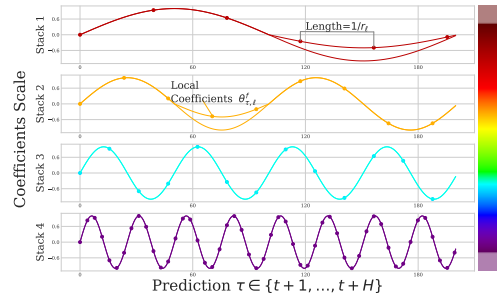


Figure 4. N-HiTS composes its predictions hierarchically using blocks specialized in different frequencies based on controlled expressiveness and interpolation of each block.

temporal interpolation via the interpolation function  $g$ :

$$\begin{aligned} \hat{y}_{\tau,\ell} &= g(\tau, \theta_\ell^f), \quad \forall \tau \in \{t+1, \dots, t+H\}, \\ \tilde{y}_{\tau,\ell} &= g(\tau, \theta_\ell^b), \quad \forall \tau \in \{t-L, \dots, t\}. \end{aligned} \quad (3)$$

The interpolation function can vary in *smoothness*,  $g \in \mathcal{C}^0, \mathcal{C}^1, \mathcal{C}^2$ . For concreteness, the linear interpolator  $g \in \mathcal{C}^1$ , depicted in Fig. 3, is defined as

$$\begin{aligned} g(\tau, \theta) &= \theta[t_1] + \left( \frac{\theta[t_2] - \theta[t_1]}{t_2 - t_1} \right) (\tau - t_1), \\ \mathcal{T} &= \{t+1, t+1+1/r_\ell, \dots, t+H-1/r_\ell, t+H\}, \\ t_1 &= \arg \min_{t \in \mathcal{T}: t \leq \tau} \tau - t, \quad t_2 = t_1 + 1/r_\ell. \end{aligned}$$

In Appendix A.4.1 we explore the nearest neighbor, piecewise linear and cubic alternatives.

Furthermore, the *hierarchical* interpolation principle is implemented by distributing expressiveness ratios across blocks in a manner synchronized with multi-rate sampling. Blocks closer to the input have smaller  $r_\ell$  and larger  $k_\ell$ , implying that input blocks generate low-granularity signals via more aggressive interpolation, being also forced to look at more aggressively sub-sampled (and smoothed) signals. The resulting hierarchical forecast is assembled by summing the outputs of all blocks, essentially composing it out of interpolations at different time-scale hierarchy levels:

$$\hat{\mathbf{y}}_{t+1:t+H} = \sum_{\ell=1}^L \hat{\mathbf{y}}_{t+1:t+H,\ell}$$

Since each block specializes on its own scale of input and output signal, this induces a clearly structured hierarchy of interpolation granularity, the intuition conveyed in Fig. 4. We propose to use *exponentially increasing expressiveness ratios* to handle a wide range of frequency bands while controlling the number of parameters. Alternatively, each stack can specialize in modeling a different known cycle of the time-series (weekly, daily etc.) using a matching  $r_\ell$

Table 1. Summary of datasets used in our empirical study. We report the train, validation and test partition.

DATASET	FREQUENCY	SERIES	TOTAL SERIES' OBSERVATIONS	VALIDATION SERIES' OBSERVATIONS	TEST SERIES' OBSERVATIONS	HORIZON ( $H$ )
ETTm <sub>2</sub>	15 MINUTE	7	57,600	11,520	11,520	{96, 192, 336, 720}
EXCHANGE	DAILY	8	7,588	760	1,517	{96, 192, 336, 720}
ECL	HOURLY	321	26,304	2,632	5,260	{96, 192, 336, 720}
TRAFFICL	HOURLY	862	17,544	1,756	3,508	{96, 192, 336, 720}
WEATHER	10 MINUTE	21	52,695	5,270	10,539	{96, 192, 336, 720}
ILI	WEEKLY	7	966	97	193	{24, 36, 48, 60}

(see Appendix A.3). Finally, the backcast residual formed at previous hierarchy scale is subtracted from the input of the next hierarchy level to amplify the focus of the next level block on signals outside of the band that has already been handled by the previous hierarchy members:

$$\mathbf{y}_{t-L:t,\ell+1} = \mathbf{y}_{t-L:t,\ell} - \tilde{\mathbf{y}}_{t-L:t,\ell}$$

## 4. Experimental Results

In this section we present our empirical results. We first describe datasets, baselines and metrics used for the quantitative evaluation of our model. Table 2 presents our key results, demonstrating SoTA performance of our method relative to existing work. We then carefully describe the details of training and evaluation setups. We conclude the section by describing the ablation studies we conducted.

### 4.1. Datasets

All large-scale datasets used in our empirical studies are publicly available<sup>1</sup> and have been used in neural forecasting literature, particularly in the context of long-horizon (Lai et al., 2017; Zhou et al., 2019; Li et al., 2019; Wu et al., 2021). Tab. 1 summarizes their characteristics. Each set is normalized with the train data mean and standard deviation.

**Electricity Transformer Temperature.** The ETTm<sub>2</sub> dataset measures an electricity transformer from a region of a province of China including oil temperature and variants of load (such as high useful load and high useless load) from July 2016 to July 2018 at a fifteen minutes frequency.

**Exchange-Rate.** The Exchange dataset is a collection of daily exchange rates of eight countries relative to the US dollar. The countries include Australia, UK, Canada, Switzerland, China, Japan, New Zealand and Singapore from 1990 to 2016.

**Electricity.** The ECL dataset reports the fifteen minute

<sup>1</sup>ETTm<sub>2</sub> is available at the [Informer's repository](#). Exchange is available at the [LSTNet's dataset repository](#). ECL is available at the [UCI ML repository](#). TrafficL is reported by the [California Department of Transportation](#). Weather is published by [Max Planck Institute](#). ILI, is reported by the [US Centers for Disease Control and Prevention](#).

electricity consumption (KWh) of 321 customers from 2012 to 2014. For comparability, we aggregate it hourly.

**San Francisco Bay Area Highway Traffic.** This TrafficL dataset was collected by the California Department of Transportation, it reports road hourly occupancy rates of 862 sensors, from January 2015 to December 2016.

**Weather.** This Weather dataset contains the 2020 year of 21 meteorological measurements recorded every 10 minutes from the Weather Station of the Max Planck Biogeochemistry Institute in Jena, Germany.

**Influenza-like illness.** The ILI dataset reports weekly recorded influenza-like illness (ILI) patients from Centers for Disease Control and Prevention of the United States from 2002 to 2021. It is measured as a ratio of ILI patients versus the total patients in the week.

### 4.2. Evaluation Setup

We evaluate the accuracy of our approach using *mean absolute error* (MAE) and *mean squared error* (MSE) metrics, which are well-established in the literature (Zhou et al., 2020; Wu et al., 2021), for varying horizon lengths  $H$ :

$$\text{MSE} = \frac{1}{H} \sum_{\tau=t}^{t+H} (\mathbf{y}_\tau - \hat{\mathbf{y}}_\tau)^2, \quad \text{MAE} = \frac{1}{H} \sum_{\tau=t}^{t+H} |\mathbf{y}_\tau - \hat{\mathbf{y}}_\tau|.$$

Note that for multivariate datasets, our algorithm produces forecast for each feature in the dataset and metrics are averaged across dataset features. Since our model is univariate, each variable is predicted using only its own history,  $\mathbf{y}_{t-L:t}$ , as input<sup>2</sup>. Datasets are partitioned into train, validation and test splits. Train split is used to train model parameters, validation split is used to tune hyperparameters, and test split is used to compute metrics reported in Table 2. Fig. 1 of Appendix A.1 shows partitioning into train, validation and test splits for all datasets: seventy, ten, and twenty percent of the available observations respectively, with the exception of ETTm<sub>2</sub> that uses twenty percent as validation.

<sup>2</sup>While the inputs are univariate, we train an unique *global* model for all features in the dataset.

Table 2. Key empirical results in long-horizon forecasting setup, lower scores are better. Metrics are averaged over eight runs and standard deviation is reported in brackets, best results are highlighted in bold.

\* The automatic ARIMA model has a unique solution, for which its results do not have variance. The evident long-horizon degradation of its performance follows from compounding prediction errors.

Horizon	N-HiTS (Ours)		Autoformer		Informer		LogTrans		Reformer		DilRNN		ARIMA*		
	MSE	MAE	MSE	MAE	MSE	MAE	MSE	MAE	MSE	MAE	MSE	MAE	MSE	MAE	
ETTm2	96	<b>0.176</b> (0.003)	<b>0.255</b> (0.001)	0.255 (0.020)	0.339 (0.020)	0.365 (0.047)	0.453 (0.071)	0.768 (0.020)	0.642 (0.121)	0.658 (0.021)	0.619 (0.249)	1.161 (0.071)	0.808 (0.071)	0.225 (0.249)	0.301 (0.301)
	192	<b>0.245</b> (0.005)	<b>0.305</b> (0.002)	0.281 (0.027)	0.340 (0.025)	0.533 (0.109)	0.563 (0.050)	0.989 (0.124)	0.757 (0.049)	1.078 (0.106)	0.827 (0.012)	1.562 (0.342)	0.932 (0.090)	0.298 (0.090)	0.345 (0.345)
	336	<b>0.295</b> (0.004)	<b>0.346</b> (0.002)	0.339 (0.018)	0.372 (0.015)	1.363 (0.173)	0.887 (0.056)	1.334 (0.168)	0.872 (0.054)	1.549 (0.146)	0.972 (0.0)	1.585 (0.327)	0.952 (0.088)	0.370 (0.088)	0.386 (0.386)
	720	<b>0.401</b> (0.013)	<b>0.426</b> (0.009)	0.422 (0.015)	0.419 (0.010)	3.379 (0.143)	1.388 (0.037)	3.048 (0.140)	1.328 (0.023)	2.631 (0.126)	1.242 (0.014)	2.114 (0.280)	1.091 (0.072)	0.478 (0.072)	0.445 (0.445)
ECL	96	<b>0.147</b> (0.002)	<b>0.249</b> (0.002)	0.201 (0.003)	0.317 (0.004)	0.274 (0.004)	0.368 (0.003)	0.258 (0.002)	0.357 (0.002)	0.312 (0.003)	0.402 (0.004)	1.358 (0.134)	0.927 (0.041)	1.220 (0.120)	0.814 (0.814)
	192	<b>0.167</b> (0.005)	<b>0.269</b> (0.005)	0.222 (0.003)	0.334 (0.004)	0.296 (0.009)	0.386 (0.007)	0.266 (0.005)	0.368 (0.004)	0.348 (0.004)	0.433 (0.005)	1.352 (0.134)	0.921 (0.041)	1.264 (0.126)	0.842 (0.842)
	336	<b>0.186</b> (0.011)	<b>0.290</b> (0.011)	0.231 (0.006)	0.338 (0.004)	0.300 (0.007)	0.394 (0.004)	0.280 (0.006)	0.380 (0.006)	0.350 (0.001)	0.433 (0.004)	1.255 (0.069)	0.896 (0.027)	1.311 (0.111)	0.866 (0.866)
	720	<b>0.243</b> (0.008)	<b>0.340</b> (0.007)	0.254 (0.007)	0.361 (0.008)	0.373 (0.034)	0.439 (0.024)	0.283 (0.003)	0.376 (0.002)	0.340 (0.002)	0.42 (0.002)	1.231 (0.165)	0.890 (0.062)	1.364 (0.136)	0.891 (0.891)
Exchange	96	<b>0.092</b> (0.002)	<b>0.211</b> (0.002)	0.197 (0.019)	0.323 (0.012)	0.847 (0.150)	0.752 (0.060)	0.968 (0.177)	0.812 (0.027)	1.065 (0.070)	0.829 (0.013)	1.945 (0.390)	1.117 (0.110)	0.296 (0.110)	0.214 (0.214)
	192	<b>0.208</b> (0.025)	<b>0.322</b> (0.020)	0.300 (0.020)	0.369 (0.016)	1.204 (0.149)	0.895 (0.061)	1.040 (0.232)	0.851 (0.029)	1.188 (0.041)	0.906 (0.008)	1.753 (0.494)	1.061 (0.150)	1.056 (0.156)	0.326 (0.326)
	336	<b>0.371</b> (0.042)	<b>0.443</b> (0.030)	0.509 (0.041)	0.524 (0.016)	1.672 (0.036)	1.036 (0.014)	1.659 (0.122)	1.081 (0.015)	1.357 (0.027)	0.976 (0.010)	1.666 (0.360)	1.044 (0.093)	2.298 (0.093)	0.467 (0.467)
	720	<b>0.888</b> (0.041)	<b>0.723</b> (0.013)	1.447 (0.084)	0.941 (0.084)	2.478 (0.198)	1.310 (0.070)	1.941 (0.327)	1.127 (0.030)	1.510 (0.071)	1.016 (0.008)	3.128 (0.561)	1.456 (0.146)	20.666 (0.146)	0.864 (0.864)
TrafficI	96	<b>0.402</b> (0.005)	<b>0.282</b> (0.002)	0.613 (0.028)	0.388 (0.012)	0.719 (0.150)	0.391 (0.060)	0.684 (0.177)	0.384 (0.027)	0.732 (0.070)	0.423 (0.013)	1.638 (0.390)	0.893 (0.110)	1.997 (0.110)	0.924 (0.924)
	192	<b>0.420</b> (0.002)	<b>0.297</b> (0.003)	0.616 (0.042)	0.382 (0.020)	0.696 (0.050)	0.379 (0.023)	0.685 (0.055)	0.39 (0.021)	0.733 (0.013)	0.42 (0.011)	1.673 (0.035)	0.899 (0.016)	2.044 (0.116)	0.944 (0.944)
	336	<b>0.448</b> (0.006)	<b>0.313</b> (0.003)	0.622 (0.009)	0.337 (0.009)	0.777 (0.003)	0.420 (0.069)	0.733 (0.026)	0.408 (0.008)	0.742 (0.012)	0.42 (0.0)	1.745 (0.043)	0.926 (0.020)	2.096 (0.020)	0.960 (0.960)
	720	<b>0.539</b> (0.022)	<b>0.353</b> (0.012)	0.660 (0.025)	0.408 (0.015)	0.864 (0.026)	0.472 (0.015)	0.717 (0.030)	0.396 (0.010)	0.755 (0.023)	0.423 (0.014)	1.927 (0.103)	0.993 (0.043)	2.138 (0.143)	0.971 (0.971)
Weather	96	<b>0.158</b> (0.002)	<b>0.195</b> (0.007)	0.266 (0.006)	0.336 (0.013)	0.300 (0.013)	0.384 (0.013)	0.458 (0.143)	0.49 (0.038)	0.689 (0.042)	0.596 (0.019)	0.477 (0.061)	0.501 (0.046)	0.217 (0.146)	0.258 (0.146)
	192	<b>0.211</b> (0.011)	<b>0.247</b> (0.003)	0.307 (0.024)	0.367 (0.022)	0.598 (0.045)	0.544 (0.028)	0.658 (0.151)	0.589 (0.032)	0.752 (0.048)	0.638 (0.029)	0.546 (0.045)	0.547 (0.034)	0.263 (0.148)	0.299 (0.148)
	336	<b>0.274</b> (0.009)	<b>0.300</b> (0.008)	0.359 (0.035)	0.395 (0.031)	0.578 (0.024)	0.523 (0.016)	0.797 (0.034)	0.652 (0.019)	0.664 (0.030)	0.596 (0.021)	0.609 (0.052)	0.584 (0.032)	0.330 (0.142)	0.347 (0.147)
	720	<b>0.351</b> (0.020)	<b>0.353</b> (0.016)	0.419 (0.017)	0.428 (0.014)	1.059 (0.096)	0.741 (0.042)	0.869 (0.045)	0.675 (0.093)	1.130 (0.084)	0.792 (0.055)	0.620 (0.042)	0.602 (0.028)	0.425 (0.146)	0.405 (0.146)
TLI	24	<b>1.862</b> (0.064)	<b>0.869</b> (0.020)	3.483 (0.107)	1.287 (0.018)	5.764 (0.354)	1.677 (0.080)	4.480 (0.313)	1.444 (0.033)	4.4 (0.177)	1.382 (0.021)	6.226 (0.809)	1.793 (0.172)	5.554 (0.172)	1.434 (1.434)
	36	<b>2.071</b> (0.015)	<b>0.969</b> (0.003)	3.103 (0.139)	1.148 (0.025)	4.755 (0.248)	1.467 (0.067)	4.799 (0.251)	1.467 (0.023)	4.783 (0.138)	1.448 (0.023)	6.019 (0.694)	1.802 (0.148)	6.940 (0.148)	1.676 (1.676)
	48	<b>2.346</b> (0.142)	<b>1.042</b> (0.034)	2.669 (0.151)	1.085 (0.037)	4.763 (0.295)	1.469 (0.059)	4.800 (0.233)	1.468 (0.021)	4.832 (0.122)	1.465 (0.016)	5.356 (0.521)	1.662 (0.114)	7.192 (0.114)	1.736 (1.736)
	60	<b>2.560</b> (0.075)	<b>1.073</b> (0.012)	2.770 (0.085)	1.125 (0.019)	5.264 (0.237)	1.564 (0.044)	5.278 (0.231)	1.56 (0.014)	4.882 (0.123)	1.483 (0.016)	5.866 (0.553)	1.728 (0.115)	6.648 (0.115)	1.656 (1.656)

### 4.3. Key Results

We compare N-HiTS to the following SoTA multivariate baselines: Autoformer (Wu et al., 2021), Informer (Zhou et al., 2020), Reformer (Kitaev et al., 2020) and LogTrans (Li et al., 2019). Additionally, we consider the univariate baselines: DilRNN (Chang et al., 2017) and auto-ARIMA (Hyndman & Khandakar, 2008).

**Forecasting Accuracy.** Table 2 summarizes the multivariate forecasting results. N-HiTS outperforms the best baseline, with average relative error decrease across datasets and horizons of 18% in MAE and 25% in MSE. N-HiTS maintains a comparable performance to other state-of-the-art methods for the shortest measured horizon (96/24), while for the longest measured horizon (720/60) decreases multivariate MAE by 11% and MSE by 17%. We complement

the key results in Table 2, with the additional univariate forecasting experiments in Appendix A.6, on the ETTm<sub>2</sub> and Exchange datasets, again demonstrating state-of-the-art performance against Transformer-based baselines.

**Computational Efficiency.** We measure the computational training time of N-HiTS, N-BEATS and Transformer-based methods in the multivariate setting and show the comparison in Figure 5. The experiment monitors the whole training process for the ETTm<sub>2</sub> dataset. For the Transformer-based models we used hyperparameters reported in (Wu et al., 2021). Compared to the Transformer-based methods, N-HiTS is the most efficient, as in the long-horizon setting, it is 45× faster than Autoformer. In terms of memory, N-HiTS also has favorable results as it scales linearly with respect to the input’s length and achieves state-of-the-art results with less than 26% of the parameters of the second-

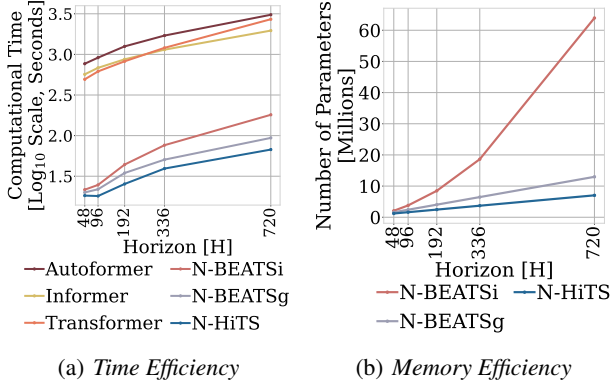


Figure 5. Computational efficiency comparison. N-HiTS exhibits the best training time compared to Transformer-based and fully connected models, as well as the smallest memory footprint.

best alternative. Compared to the original N-BEATS, our method is  $1.26 \times$  faster and requires only 54% of the parameters. We explore this in more detail in Appendix A.5.

#### 4.4. Training and Hyperparameter Optimization

Table 3. Considered hyperparameters for N-HiTS.

HYPERPARAMETER	CONSIDERED VALUES
Initial learning rate.	{1e-3}
Training steps.	{1000}
Random seed for initialization.	DiscreteRange(1, 10)
Input size multiplier ( $L=m^*H$ ).	$m \in \{5\}$
Batch Size.	{256}
Activation Function.	ReLU
Learning rate decay (3 times).	0.5
Pooling Kernel Size.	$[k_1, k_2, k_3] \in \{[2,2,2], [4,4,4], [8,8,8], [8,4,1], [16,8,1]\}$
Number of Stacks.	$S \in \{3\}$
Number of Blocks in each stack.	$B \in \{1\}$
MLP Layers.	{2}
Coefficients Hidden Size.	$N_h \in \{512\}$
Number of Stacks' Coefficients.	$[r_1^{-1}, r_2^{-1}, r_3^{-1}] \in \{[168,24,1], [24,12,1], [180,60,1], [40,20,1], [64,8,1]\}$
Interpolation strategy	$g(\tau, \theta) \in \{\text{Linear}\}$

We consider a minimal space of hyperparameters for optimization to explore configurations of the N-HiTS architecture. First, we consider the kernel pooling size for multi-rate sampling from Equation (1). Second, the number of coefficients from Equation (2) that we selected between several alternatives, some matching common seasonalities of the datasets and others exponentially increasing. We tune the random seed to escape underperforming local minima. Other details are reported in Appendix A.2.

During the *hyperparameter optimization phase*, we measure MAE performance on the validation set and use a Bayesian optimization library (HYPEROPT; Bergstra et al. 2011), with 20 iterations. We use the optimal configuration based on the validation loss to make prediction on the

test set. We refer to the combination of hyperparameter optimization and test prediction as a *run*.

N-HiTS is implemented in PyTorch (Paszke et al., 2019) and trained using ADAM optimizer (Kingma & Ba, 2014), MAE loss, batch size 256 and initial learning rate of 1e-3, halved three times across the training procedure. All our experiments are conducted on a GeForce RTX 2080 GPU.

#### 4.5. Ablation Studies

We believe that the advantages of the N-HiTS architecture are rooted in its multi-rate hierarchical nature. Fig. 6 shows a qualitative comparison of N-HiTS with and without hierarchical interpolation/multi-rate sampling components. We clearly see N-HiTS developing the ability to produce interpretable forecast decomposition providing valuable information about trends and seasonality in separate channels, unlike the control model. Continuing this line of investigation, we support our qualitative conclusion with quantitative results. We define the following set of alternative models: N-HiTS, our proposed model with both multi-rate sampling and hierarchical interpolation, N-HiTS<sub>2</sub> only hierarchical interpolation, N-HiTS<sub>3</sub> only multi-rate sampling, N-HiTS<sub>4</sub> no multi-rate sampling or interpolation (corresponds to the original N-BEATSg (Oreshkin et al., 2020)), finally N-BEATSi, the interpretable version of the N-BEATS ((Oreshkin et al., 2020)). Tab. 4 clearly shows that the combination of both proposed components (hierarchical interpolation and multi-rate sampling) results in the best performance, emphasizing their complementary nature in long-horizon forecasting. We see that the original N-BEATS is consistently worse, especially the N-BEATSi.

Additional ablation studies are reported in Appendix A.4. The MaxPool multi-rate sampling wins over AveragePool (see Appendix A.4.2). Linear interpolation wins over nearest neighbor and cubic (see Appendix A.4.1). Finally and most importantly, in Appendix A.4.3 we show that the order in which hierarchical interpolation is implemented matters significantly. The best configuration is to have the low-frequency/large-scale components synthesized and removed from analysis first, followed by more fine-grained modeling of high-frequency/intermittent signals.

## 5. Discussion of Findings

Our results indicate the complementarity and effectiveness of multi-rate sampling and hierarchical interpolation in the context of long-horizon time-series forecasting. Table 4 indicates that these components enforce a useful inductive bias compared to both the free-form model N-HiTS<sub>4</sub> (plain fully connected architecture) and the parametric model N-BEATSi (polynomial trend and sinusoidal seasonality used as basis functions in two respective stacks). The latter

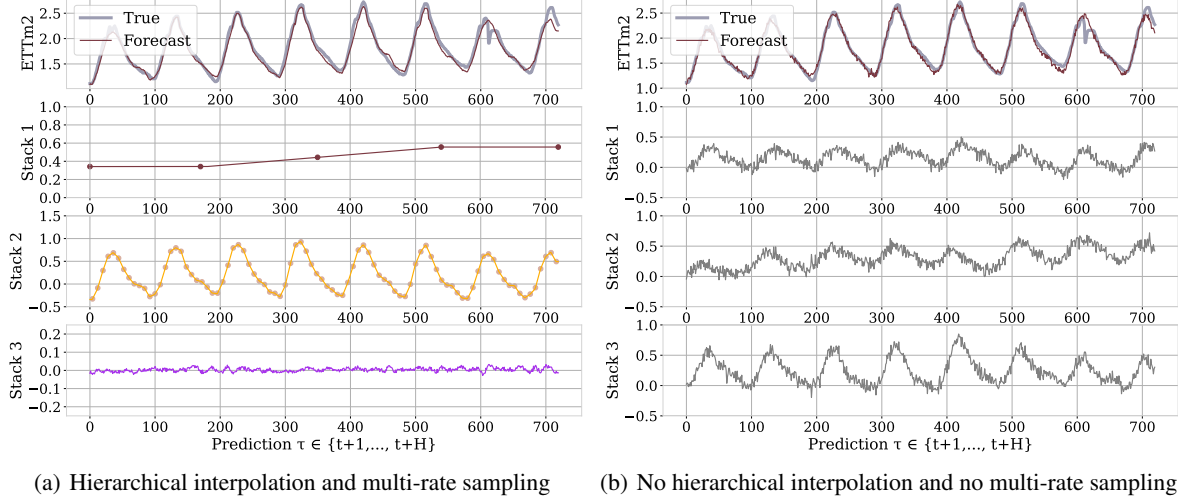


Figure 6. ETTm2 and 720 ahead forecasts using N-HiTS (left panel), N-HiTS with hierarchical interpolation and multi-rate sampling removed (right panel). The top row shows the original signal and the forecast. The second, third and fourth rows show the forecast components for each stack. In (a), each block shows scale specialization, unlike (b), in which signals are not interpretable.

Table 4. Empirical evaluation of long multi-horizon multivariate forecasts for N-HiTS with/without enhancements. MAE and MSE for predictions averaged over eight runs, and five datasets, the best result is highlighted in bold, second best in blue (lower is better).

	N-HiTS	N-HiTS <sub>2</sub>	N-HiTS <sub>3</sub>	N-HiTS <sub>4</sub>	N-BEATSI
A. MSE	96	<b>0.195</b>	0.196	<b>0.192</b>	0.196
	192	<b>0.250</b>	0.261	<b>0.251</b>	0.263
	336	<b>0.315</b>	<b>0.315</b>	0.342	0.346
	720	<b>0.484</b>	<b>0.498</b>	0.518	0.548
A. MAE	96	<b>0.239</b>	0.241	<b>0.237</b>	0.240
	192	<b>0.290</b>	0.299	<b>0.291</b>	0.300
	336	<b>0.338</b>	<b>0.342</b>	0.346	0.352
	720	<b>0.439</b>	<b>0.450</b>	0.454	0.468

obviously providing a detrimental inductive bias for long-horizon forecasting. Notwithstanding our current success, we believe we barely scratched the surface in the right direction and further progress is possible using advanced multi-scale processing approaches in the context of time-series forecasting, motivating further research.

N-HiTS outperforms SoTA baselines while simultaneously providing an interpretable non-linear decomposition. Fig. 1 showcases N-HiTS perfectly reconstructing latent harmonic signals from synthetic data, revealing frequency specialization in stacks. Fig. 6 shows N-HiTS decomposing real data. This novel interpretable decomposition can provide additional insights to users and improve their confidence in high-stakes applications such as in healthcare.

In this work *expressiveness ratio* schedules are motivated by seasonalities and geometric decay. It would be of interest to develop a theoretical guide to support this design. For example, Nyquist-Shannon rates could define bandwidths associated with N-HiTS stacks, that effectively

work as neural filters (Marks, 1991).

Our study raises a question about the effectiveness of the existing long-horizon multi-variate forecasting approaches, given that all of them are substantially outperformed by our univariate algorithm. If these approaches underperform due to problems with overfitting and model parsimony at the level of marginals, it is likely that the integration of our approach with Transformer-inspired architectures could form a promising research direction. Univariate results in Appendix A.6 suggest that it might be the case. However, there is also a chance that the existing approaches underperform due to their inability to effectively integrate information from multiple variables, which clearly hints at possibly untapped research potential in this area. Whichever is the case, we believe our results provide a strong guidance signal and a valuable baseline for future research in the area of long-horizon multi-variate forecasting.

## 6. Conclusions

We proposed a novel neural forecasting algorithm N-HiTS that combines two complementary techniques, multi-rate input sampling and hierarchical interpolation, to produce drastically improved, interpretable and computationally efficient long-horizon time-series predictions. Our model, operating in the univariate regime and accepting only the predicted time-series' history, significantly outperforms all previous Transformer-based multi-variate models using an order of magnitude less computation. This sets a new baseline for all ensuing multi-variate work on six popular datasets and motivates further research to find models that are able to effectively use information from multiple variables.

## References

Alaa, A. M. and van der Schaar, M. Attentive state-space modeling of disease progression. In Wallach, H., Larochelle, H., Beygelzimer, A., d'Alché-Buc, F., Fox, E., and Garnett, R. (eds.), *33rd Conference on Neural Information Processing Systems (NeurIPS 2019)*, volume 32. Curran Associates, Inc., 2019. URL <https://proceedings.neurips.cc/paper/2019/file/1d0932d7f57ce74d9d9931a2c6db8a06-Paper.pdf>.

Armesto, M. T., Engemann, K. M., and Owyang, M. T. Forecasting with mixed frequencies. *Federal Reserve Bank of St. Louis Review*, 92:521–536, 2010. URL <https://research.stlouisfed.org/publications/review/2010/11/01/forecasting-with-mixed-frequencies>.

Atiya, A. and Taieb, B. A bias and variance analysis for multistep-ahead time series forecasting. *IEEE transactions on neural networks and learning systems*, 27(1):2162–2388, 2016. URL <https://pubmed.ncbi.nlm.nih.gov/25807572/>.

Banushev, B. and Barclay, R. Enhancing trading strategies through cloud services and machine learning, Jan 2021. URL <https://aws.amazon.com/blogs/industries>.

Bao, Y., Xiong, T., and Hu, Z. Multi-step-ahead time series prediction using multiple-output support vector regression. *Neurocomputing*, 129:482–493, 2014. ISSN 0925-2312. doi: <https://doi.org/10.1016/j.neucom.2013.09.010>. URL <https://www.sciencedirect.com/science/article/pii/S092523121300917X>.

Basher, R. Global early warning systems for natural hazards: Systematic and people-centred. *Philosophical transactions. Series A, Mathematical, physical, and engineering sciences*, 364:2167–82, 09 2006. doi: 10.1098/rsta.2006.1819.

Bengio, Y., Courville, A. C., and Vincent, P. Unsupervised feature learning and deep learning: A review and new perspectives. *CoRR*, abs/1206.5538, 2012. URL <http://arxiv.org/abs/1206.5538>.

Benidis, K., Rangapuram, S. S., Flunkert, V., Wang, B., Maddix, D., Turkmen, C., Gasthaus, J., Bohlke-Schneider, M., Salinas, D., Stella, L., Callot, L., and Januschowski, T. Neural forecasting: Introduction and literature overview. *Computing Research Repository*, 2020.

Bergstra, J., Bardenet, R., Bengio, Y., and Kégl, B. Algorithms for hyper-parameter optimization. In Shawe-Taylor, J., Zemel, R., Bartlett, P., Pereira, F., and Weinberger, K. Q. (eds.), *Advances in Neural Information Processing Systems*, volume 24, pp. 2546–2554. Curran Associates, Inc., 2011. URL <https://proceedings.neurips.cc/paper/2011/file/86e8f7ab32cf12577bc2619bc635690-Paper.pdf>.

Chang, S., Zhang, Y., Han, W., Yu, M., Guo, X., Tan, W., Cui, X., Witbrock, M., Hasegawa-Johnson, M. A., and Huang, T. S. Dilated recurrent neural networks. In Guyon, I., Luxburg, U. V., Bengio, S., Wallach, H., Fergus, R., Vishwanathan, S., and Garnett, R. (eds.), *Advances in Neural Information Processing Systems*, volume 30. Curran Associates, Inc., 2017. URL <https://proceedings.neurips.cc/paper/2017/file/32bb90e8976aab5298d5da10fe66f21d-Paper.pdf>.

Child, R., Gray, S., Radford, A., and Sutskever, I. Generating long sequences with Sparse Transformers. *CoRR*, abs/1904.10509, 2019. URL <http://arxiv.org/abs/1904.10509>.

Chow, G. C. and loh Lin, A. Best linear unbiased interpolation, distribution, and extrapolation of time series by related series. *The Review of Economics and Statistics*, 53(4):372–375, 1971. ISSN 00346535, 15309142. URL <http://www.jstor.org/stable/1928739>.

Churpek, M. M., Adhikari, R., and Edelson, D. P. The value of vital sign trends for detecting clinical deterioration on the wards. *Resuscitation*, 102:1–5, 2016.

Fan, C., Zhang, Y., Pan, Y., Li, X., Zhang, C., Yuan, R., Wu, D., Wang, W., Pei, J., and Huang, H. Multi-horizon time series forecasting with temporal attention learning. In *Proceedings of the 25th ACM SIGKDD International Conference on Knowledge Discovery & Data Mining*, KDD '19, pp. 2527–2535, New York, NY, USA, 2019. Association for Computing Machinery. ISBN 9781450362016. doi: 10.1145/3292500.3330662. URL <https://doi.org/10.1145/3292500.3330662>.

Fernandez, R. B. A Methodological Note on the Estimation of Time Series. *The Review of Economics and Statistics*, 63(3):471–476, August 1981. URL <https://ideas.repec.org/a/tpr/restat/v63y1981i3p471-76.html>.

Field, C. B., Barros, V., Stocker, T. F., and Dahe, Q. *Managing the risks of extreme events and disasters to advance climate change adaptation: special report of the intergovernmental panel on climate change*. Cambridge University Press, 2012.

Gasthaus, J., Benidis, K., Wang, B., Rangapuram, S. S., Salinas, D., Flunkert, V., and Januschowski, T. Probabilistic forecasting with spline quantile function rnns. In *AISTATS*, 2019.

Ghysels, E., Sinko, A., and Valkanov, R. Midas regressions: Further results and new directions. *Econometric Reviews*, 26(1):53–90, 2007. doi: 10.1080/07474930600972467. URL <https://doi.org/10.1080/07474930600972467>.

Hyndman, R. J. and Fan, S. Density forecasting for long-term peak electricity demand. *IEEE Transactions on Power Systems*, 25(2):1142–1153, 2009.

Hyndman, R. J. and Khandakar, Y. Automatic time series forecasting: The forecast package for r. *Journal of Statistical Software, Articles*, 27(3):1–22, 2008. ISSN 1548-7660. doi: 10.18637/jss.v027.i03. URL <https://www.jstatsoft.org/v027/i03>.

Kingma, D. P. and Ba, J. ADAM: A method for stochastic optimization, 2014. URL <http://arxiv.org/abs/1412.6980>. cite arxiv:1412.6980Comment: Published as a conference paper at the 3rd International Conference for Learning Representations (ICLR), San Diego, 2015.

Kitaev, N., Łukasz Kaiser, and Levskaya, A. Reformer: The Efficient Transformer. In *8th International Conference on Learning Representations, (ICLR 2020)*, 2020. URL <https://arxiv.org/abs/2001.04451>.

Lai, G., Chang, W., Yang, Y., and Liu, H. Modeling Long- and Short-Term Temporal Patterns with Deep Neural Networks. *Special Interest Group on Information Retrieval Conference 2018 (SIGIR 2018)*, abs/1703.07015, 2017. URL <http://arxiv.org/abs/1703.07015>.

Laptev, N., Yosinsk, J., Erran, L. L., and Smyl, S. Time-series extreme event forecasting with neural networks at UBER. In *34th International Conference on Machine Learning ICML 2017, Time Series Workshop*, 2017. URL [http://www.cs.columbia.edu/~lierranli/publications/TSW2017\\_paper.pdf](http://www.cs.columbia.edu/~lierranli/publications/TSW2017_paper.pdf).

Li, S., Jin, X., Xuan, Y., Zhou, X., Chen, W., Wang, Y., and Yan, X. Enhancing the locality and breaking the memory bottleneck of Transformer on time series forecasting. In Wallach, H., Larochelle, H., Beygelzimer, A., d’Alché-Buc, F., Fox, E., and Garnett, R. (eds.), *33rd Conference on Neural Information Processing Systems (NeurIPS 2019)*, volume 32. Curran Associates, Inc., 2019. URL <http://arxiv.org/abs/1907.00235>.

Lim, B., Arik, S. Ö., Loeff, N., and Pfister, T. Temporal Fusion Transformers for interpretable multi-horizon time series forecasting. *International Journal of Forecasting*, 2021. URL <https://arxiv.org/abs/1912.09363>.

Makridakis, S., Spiliotis, E., and Assimakopoulos, V. The M4 competition: 100,000 time series and 61 forecasting methods. *International Journal of Forecasting*, 36(1):54–74, 2020. ISSN 0169-2070. doi: <https://doi.org/10.1016/j.ijforecast.2019.04.014>. URL <https://www.sciencedirect.com/science/article/pii/S0169207019301128>. M4 Competition.

Makridakis, S., Spiliotis, E., and Assimakopoulos, V. Predicting/hypothesizing the findings of the M5 competition. *International Journal of Forecasting*, 2021. ISSN 0169-2070. doi: <https://doi.org/10.1016/j.ijforecast.2021.09.014>. URL <https://www.sciencedirect.com/science/article/pii/S0169207021001631>.

Marcellino, M., Stock, J. H., and Watson, M. W. A comparison of direct and iterated multistep ar methods for forecasting macroeconomic time series. *Journal of Econometrics*, 135(1):499–526, 2006. ISSN 0304-4076. doi: <https://doi.org/10.1016/j.jeconom.2005.07.020>. URL <https://www.sciencedirect.com/science/article/pii/S030440760500165X>.

Marks, R. J. *Introduction to Shannon Sampling and Interpolation Theory*. Springer-Verlag, Berlin, Heidelberg, 1991. ISBN 0387973915.

Meijering, E. A chronology of interpolation: from ancient astronomy to modern signal and image processing. *Proceedings of the IEEE*, 90(3):319–342, 2002. doi: 10.1109/5.993400. URL <https://ieeexplore.ieee.org/document/993400>.

Olivares, K. G., Challu, C., Marcjasz, G., Weron, R., and Dubrawski, A. Neural basis expansion analysis with exogenous variables: Forecasting electricity prices with NBEATSx. *International Journal of Forecasting, submitted*, Working Paper version available at arXiv:2104.05522, 2021a. URL <https://arxiv.org/abs/2104.05522>.

Olivares, K. G., Meetei, N. O., Ma, R., Reddy, R., Cao, M., and Dicker, L. Probabilistic hierarchical forecasting with Deep Poisson Mixtures. *International Journal of Forecasting (Hierarchical Forecasting special issue), submitted*, Working Paper version available at arXiv:2110.13179, 2021b. URL <https://arxiv.org/abs/2110.13179>.

Oreshkin, B. N., Carpol, D., Chapados, N., and Bengio, Y. N-BEATS: neural basis expansion analysis for interpretable time series forecasting. In *8th International*

*Conference on Learning Representations, ICLR 2020*, 2020. URL <https://openreview.net/forum?id=r1ecqn4YwB>.

Paszke et al. Pytorch: An imperative style, high-performance Deep Learning library. In Wallach, H., Larochelle, H., Beygelzimer, A., d Alché-Buc, F., Fox, E., and Garnett, R. (eds.), *Advances in Neural Information Processing Systems 32*, pp. 8024–8035. Curran Associates, Inc., 2019.

Rubanova, Y., Chen, R. T. Q., and Duvenaud, D. Latent ODEs for irregularly-sampled time series. In *Advances in Neural Information Processing Systems 33 (NeurIPS 2019)*, 2019. URL <http://arxiv.org/abs/1907.03907>.

Salinas, D., Flunkert, V., Gasthaus, J., and Januschowski, T. DeepAR: Probabilistic forecasting with autoregressive recurrent networks. *International Journal of Forecasting*, 36(3):1181–1191, 2020. ISSN 0169-2070. doi: <https://doi.org/10.1016/j.ijforecast.2019.07.001>. URL <https://www.sciencedirect.com/science/article/pii/S0169207019301888>.

Shukla, S. N. and Marlin, B. M. Interpolation-prediction networks for irregularly sampled time series, 2019. URL <http://arxiv.org/abs/1412.6980>. cite arxiv:1412.6980Comment: Published as a conference paper at the 7th International Conference for Learning Representations (ICLR), New Orleans, 2019.

Taylor, S. J. and Letham, B. Forecasting at scale. *The American Statistician*, 72(1):37–45, 2018.

Wen, R., Torkkola, K., Narayanaswamy, B., and Madeka, D. A Multi-horizon Quantile Recurrent Forecaster. In *31st Conference on Neural Information Processing Systems NIPS 2017, Time Series Workshop*, 2017. URL <https://arxiv.org/abs/1711.11053>.

Wu, H., Xu, J., Wang, J., and Long, M. Autoformer: Decomposition Transformers with auto-correlation for long-term series forecasting. In Ranzato, M., Beygelzime, A., Liang, P., Vaughan, J., and Dauphin, Y. (eds.), *Advances in Neural Information Processing Systems 35 (NeurIPS 2021)*, 2021. URL <https://arxiv.org/abs/2106.13008>.

Zhou, H., Zhang, S., Peng, J., Zhang, S., Li, J., Xiong, H., and Zhang, W. Informer: Beyond Efficient Transformer for Long Sequence Time-Series Forecasting. *The Association for the Advancement of Artificial Intelligence Conference 2021 (AAAI 2021)*, abs/2012.07436, 2020. URL <https://arxiv.org/abs/2012.07436>.

Zhou, S., Zhou, L., Mao, M., Tai, H., and Wan, Y. An optimized heterogeneous structure LSTM network for electricity price forecasting. *IEEE Access*, 7:108161–108173, 2019. doi: 10.1109/ACCESS.2019.2932999.

Ziel, F. and Steinert, R. Probabilistic mid- and long-term electricity price forecasting. *Renewable and Sustainable Energy Reviews*, 94:251–266, 2018. URL <https://arxiv.org/abs/1703.10806>.

## A. Appendix

### A.1. Datasets' Partition

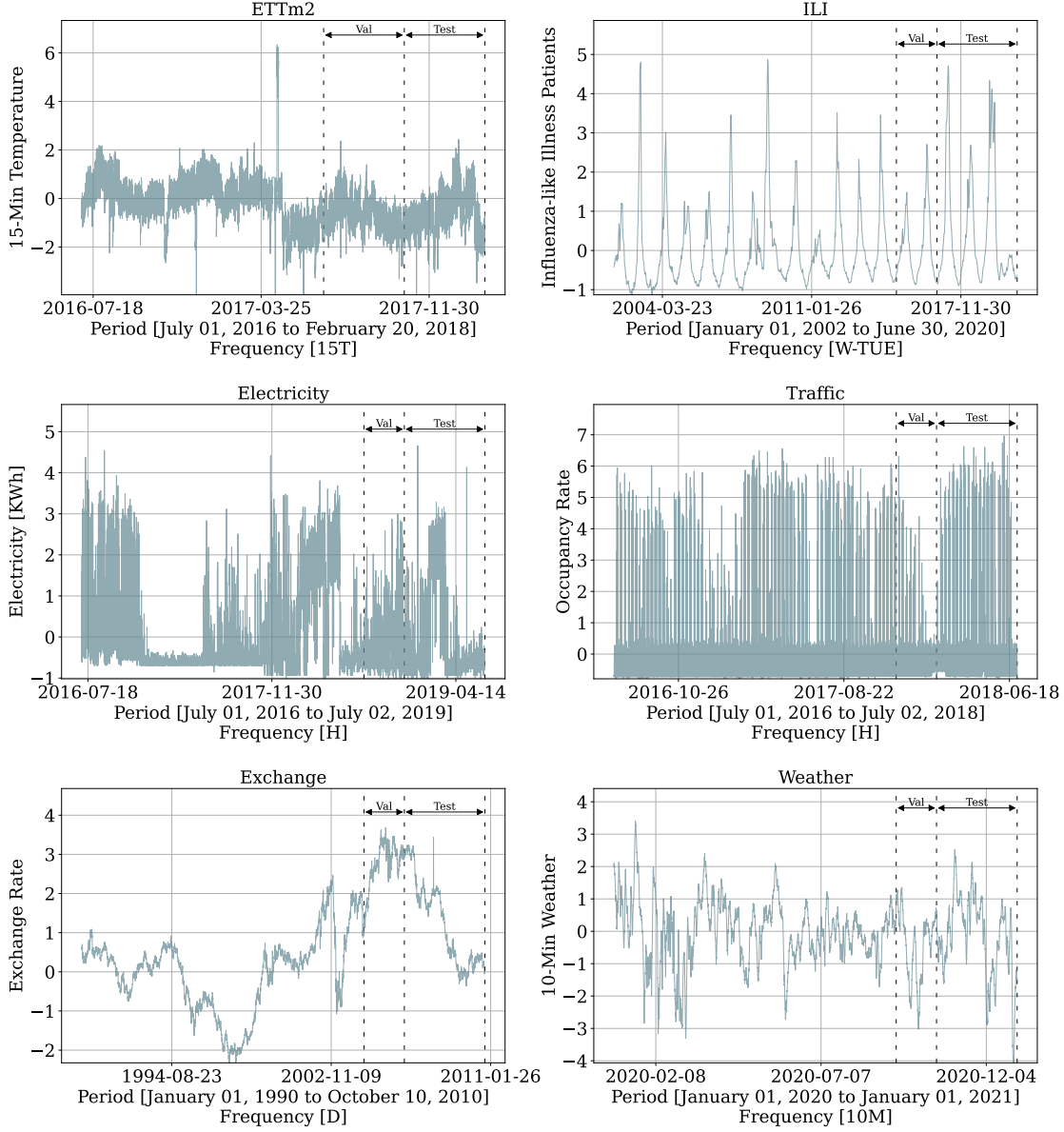


Figure 1. Datasets' partition into train, validation, and test sets used in our experiments (ETTm2, ECL, Exchange, ILI, TrafficL, and Weather). All datasets use the last 20% of the total observations as test set (marked by the second dotted line), and the 10% preceding the test set as validation (between the first and second dotted lines), except for ETTm2 that also use 20% as validation. The validation set provides the signal for hyperparameter optimization. We construct test predictions using rolling windows.

## A.2. Benchmark Hyperparameters

All benchmark neural forecasting methods optimize the length of the input  $\{96, 192, 336, 720\}$  for ETT, Weather, and ECL,  $\{24, 36, 48, 60\}$  for ILI, and  $\{24, 48, 96, 192, 288, 480, 672\}$  for ETTm. The Transformer-based models: Autoformer, Informer, LogTrans, and Reformer are trained with MSE loss and ADAM of 32 batch size, using a starting learning rate of 1e-4, halved every two epochs, for ten epochs with early stopping. Additionally, for comparability of the computational requirements, all use two encoder layers and one decoder layer.

We use the adaptation to the long-horizon time series setting provided by Wu et al. 2021 of the Reformer (Kitaev et al., 2020), and LogTrans (Li et al., 2019), with the multi-step forecasting strategy (non-dynamic decoding).

The Autoformer (Wu et al., 2021) explores with grid-search the top-k auto-correlation filter hyper-parameter in  $\{1, 2, 3, 4, 5\}$ . And fixes inputs  $L = 96$  for all datasets except for ILI in which they use  $L = 36$ . For the Informer (Zhou et al., 2020) we use the reported best hyperparameters found using an grid-search, that include dimensions of the encoder layers  $\{6, 4, 3, 2\}$ , the dimension of the decoder layer  $\{2\}$ , the heads of the multi-head attention layers  $\{8, 16\}$  and its output's dimension  $\{512\}$ .

We considered other classic models, like the automatically selected ARIMA model (Hyndman & Khandakar, 2008). The method is trained with maximum likelihood estimation under normality and independence. And integrates root statistical tests with model selection performed with Akaike's Information Criterion. For the univariate forecasting experiment we consider Prophet (Taylor & Letham, 2018), an automatic Bayesian additive regression that accounts for different frequencies non-linear trends, seasonal and holiday effects, for this method we tuned are the seasonality mode  $\{\text{multiplicative, additive}\}$ , the length of the inputs.

## A.3. Complexity Analysis

We consider a single forecast of length  $H$  for the following complexity analysis, with a N-BEATS and a N-HiTS architecture of  $B$  blocks. We do not consider the batch dimension. We consider most practical situations, the input size  $L = \mathcal{O}(H)$  linked to the horizon length.

The block operation described by Equation (2) has complexity dominated by the fully connected layers of  $\mathcal{O}(H N_h)$ , with  $N_h$  the number of hidden units that we treat as a constant. The depth of stacked blocks in the N-BEATSG architecture, that endows it with its expressivity, is associated to a computational complexity that scales linearly  $\mathcal{O}(HB)$ , with  $B$  the number of blocks.

Table A1. Computational complexity of neural based forecasting methods as a function of the output size  $H$ . For simplicity, we assume that the input size  $L$  scales linearly with respect to  $H$ . For N-HiTS and N-BEATS we also consider the network's  $B$  blocks.

MODEL	TIME	MEMORY
LSTM	$\mathcal{O}(H)$	$\mathcal{O}(H)$
ESRNN	$\mathcal{O}(H)$	$\mathcal{O}(H)$
TCN	$\mathcal{O}(H)$	$\mathcal{O}(H)$
Transformer	$\mathcal{O}(H^2)$	$\mathcal{O}(H^2)$
Reformer	$\mathcal{O}(H \log H)$	$\mathcal{O}(H \log H)$
Informer	$\mathcal{O}(H \log H)$	$\mathcal{O}(H \log H)$
Autoformer	$\mathcal{O}(H \log H)$	$\mathcal{O}(H \log H)$
LogTrans	$\mathcal{O}(H \log H)$	$\mathcal{O}(H^2)$
N-BEATSi	$\mathcal{O}(H^2 B)$	$\mathcal{O}(H^2 B)$
N-BEATSG	$\mathcal{O}(HB)$	$\mathcal{O}(HB)$
N-HiTS	$\mathcal{O}(H(1 - r^B)/(1 - r))$	$\mathcal{O}(H(1 - r^B)/(1 - r))$

The block operation described by Equation (2) has complexity dominated by the fully connected layers of  $\mathcal{O}(H N_h)$ , with  $N_h$  the number of hidden units that we treat as a constant. The depth of stacked blocks in the N-BEATSG architecture, which endows it with its expressivity, is associated with a computational complexity that scales linearly  $\mathcal{O}(HB)$ , with  $B$  the number of blocks.

In contrast the N-HiTS architecture that specializes each stack in different frequencies, through the expressivity ratios, can greatly reduce the amount of parameters needed for each layer. When we use *exponentially increasing expressivity* ratios through the depth of the architecture blocks it allows to model complex dependencies, while controlling the number of parameters used on each output layer. If the *expressivity ratio* is defined as  $r_l = r^l$  then the space complexity of N-HiTS scales geometrically  $\mathcal{O}(\sum_{l=0}^B H r^l) = \mathcal{O}((H(1 - r^B)/(1 - r))$ .

## A.4. Ablation Studies

This section performs ablation studies on the validation set of five datasets that share horizon lengths, ETTm<sub>2</sub>, Exchange, ECL, TrafficL, and Weather. The section's experiments control for N-HiTS settings described in Table 3, only varying a single characteristic of interest of the network and measuring the effects in validation.

### A.4.1. INTERPOLATION CONFIGURATIONS

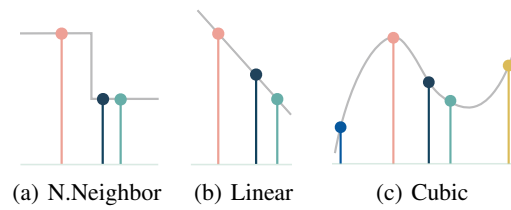


Figure 2. Proposed interpolator configurations.

In Section 3.3 we described the *hierarchical interpolation* enhancement of the multi-step prediction strategy. Here we conduct a study to compare the accuracy effects of different interpolation alternatives. To do it, we change the interpolation technique used in the multi-step forecasting strategy of the N-HiTS architecture. The interpolation techniques considered are nearest neighbor, linear and cubic. We describe them in detail below.

Recalling the notation from Section 3.3, consider the time indexes of a multi-step prediction  $\tau \in \{t+1, \dots, t+H\}$ , let  $\mathcal{T} = \{t+1, t+1+1/r_\ell, \dots, t+H\}$  be the anchored indexes in N-HiTS layer  $\ell$ , and the forecast  $\hat{y}_{\tau, \ell} = g(\tau, \theta_\ell^f)$  and backcast  $\tilde{y}_{\tau, \ell} = g(\tau, \theta_\ell^b)$  components. Here we define different alternatives for the interpolating function  $g \in \mathcal{C}^0, \mathcal{C}^1, \mathcal{C}^2$ . For simplicity we skip the  $\ell$  layer index.

**Nearest Neighbor.** In the simplest form of interpolation, we use the anchor observations in the time dimension closest to the observation we want to predict. Specifically, the prediction is defined as follows:

$$\hat{y}_\tau = \theta[t^*] \quad \text{with} \quad t^* = \operatorname{argmin}_{t \in \mathcal{T}} \{|t - \tau|\} \quad (4)$$

**Linear.** An efficient alternative is the linear interpolation method, which uses the two closest neighbor indexes  $t_1$  and  $t_2$ , and fits a linear function that passes through both.

$$\hat{y}_\tau = \left( \theta[t_1] + \left( \frac{\theta[t_2] - \theta[t_1]}{t_2 - t_1} \right) (\tau - t_1) \right) \quad (5)$$

**Cubic.** Finally we consider the Hermite cubic polynomials defined by the interpolation constraints for two anchor observations  $\theta_{t_1}$  and  $\theta_{t_2}$  and its first derivatives  $\theta'_{t_1}$  and  $\theta'_{t_2}$ .

$$\hat{y}_\tau = \theta[t_1]\phi_1(\tau) + \theta[t_2]\phi_2(\tau) + \theta'[t_1]\psi_1(\tau) + \theta'[t_2]\psi_2(\tau) \quad (6)$$

With the Hermite cubic basis defined by:

$$\phi_1(\tau) = 2\tau^3 - 3\tau^2 + 1 \quad (7a)$$

$$\phi_2(\tau) = -2\tau^3 + 3\tau^2 \quad (7b)$$

$$\psi_1(\tau) = \tau^3 - 2\tau^2 + \tau \quad (7c)$$

$$\psi_2(\tau) = \tau^3 - \tau^2 \quad (7d)$$

The ablation study results for the different interpolation techniques are summarized in Table A2, we report the average MAE and MSE performance across the five datasets.

We found that linear and cubic interpolation consistently outperform the nearest neighbor alternative, and show monotonic improvements relative to the nearest neighbor technique along the forecasting horizon.

The linear interpolation improvements over nearest neighbors are up to 15.8%, and up to 7.0% for the cubic interpolation. When comparing between linear and cubic the results

are inconclusive as different datasets and horizons slight performance differences. On average across the datasets both the forecasting accuracy and computational performance favors the linear method, with which we conducted the main experiments of this work with this technique.

Table A2. Empirical evaluation of long multi-horizon multivariate forecasts for N-HiTS with different interpolation configurations. All other hyperparameters were kept constant across all datasets. MAE and MSE for predictions averaged over eight seeds, the best result is highlighted in bold (lower is better). Percentage difference relative to n. neighbor in the last panel, average across datasets.

		Linear		Cubic		N.Neighbor	
		MSE	MAE	MSE	MAE	MSE	MAE
ETTM2	96	0.185	0.265	<b>0.179</b>	<b>0.256</b>	0.180	0.259
	192	0.244	0.308	<b>0.241</b>	<b>0.303</b>	0.252	0.315
	336	<b>0.301</b>	<b>0.347</b>	0.314	0.358	0.302	0.351
	720	<b>0.429</b>	<b>0.438</b>	0.439	0.450	0.442	0.455
ECL	96	0.152	0.257	<b>0.149</b>	<b>0.252</b>	0.151	0.255
	192	<b>0.172</b>	<b>0.275</b>	0.174	0.279	0.175	0.279
	336	0.197	0.304	<b>0.190</b>	<b>0.295</b>	0.211	0.318
	720	<b>0.248</b>	<b>0.347</b>	0.256	0.353	0.263	0.358
Exchange	96	<b>0.109</b>	<b>0.232</b>	0.1307	0.254	0.126	0.248
	192	0.280	0.375	<b>0.247</b>	<b>0.357</b>	0.357	0.416
	336	<b>0.472</b>	<b>0.504</b>	0.625	0.560	0.646	0.560
	720	<b>1.241</b>	<b>0.823</b>	1.539	0.925	1.740	0.973
TrafficL	96	0.405	0.286	<b>0.402</b>	<b>0.282</b>	0.405	0.359
	192	0.421	0.297	<b>0.417</b>	<b>0.295</b>	0.419	0.201
	336	0.448	0.318	<b>0.446</b>	<b>0.315</b>	0.445	0.253
	720	0.527	0.362	0.540	0.366	<b>0.525</b>	<b>0.318</b>
Weather	96	0.164	0.199	0.162	0.203	<b>0.161</b>	0.360
	192	0.224	0.255	0.225	0.257	<b>0.218</b>	0.928
	336	<b>0.285</b>	<b>0.311</b>	0.285	0.304	0.298	0.988
	720	<b>0.366</b>	<b>0.359</b>	0.380	0.369	0.368	1.047
P. Diff.	96	<b>-0.907</b>	<b>-0.717</b>	0.146	1.61	0.000	0.000
	192	-5.582	-3.259	<b>-7.985</b>	<b>-4.332</b>	0.000	0.000
	336	<b>-10.516</b>	<b>-4.199</b>	-2.108	-1.455	0.000	0.000
	720	<b>-15.800</b>	<b>-7.042</b>	-5.480	-1.579	0.000	0.000

#### A.4.2. POOLING CONFIGURATIONS

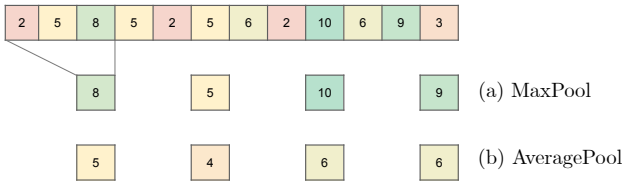


Figure 3. Proposed pooling configurations.

In Section 3.1 we described the *multi-rate signal sampling* enhancement of the N-HiTS architecture. Here we conduct a study to compare the accuracy effects of different pooling alternatives, on Equation (1). We consider the MaxPool and AveragePool configurations.

As shown in Table A3, the MaxPool operation consistently outperforms the AveragePool alternative, with MAE improvements up to 15% and MSE up to 8% in the most extended horizon. On average, the forecasting accuracy favors the MaxPool method across the datasets and horizons.

**Table A3.** Empirical evaluation of long multi-horizon multivariate forecasts for N-HiTS with different pooling configurations. All other hyperparameters were kept constant across all datasets. MAE and MSE for predictions averaged over eight seeds, the best result is highlighted in bold (lower is better). Average percentage difference relative to average pooling in the last panel.

		MaxPool		AveragePool	
		MSE	MAE	MSE	MAE
ETTm2	96	<b>0.185</b>	0.265	0.186	<b>0.262</b>
	192	<b>0.244</b>	<b>0.308</b>	0.257	0.315
	336	<b>0.301</b>	<b>0.347</b>	0.312	0.356
	720	<b>0.429</b>	<b>0.438</b>	0.436	0.447
ECL	96	<b>0.152</b>	<b>0.257</b>	0.181	0.290
	192	<b>0.172</b>	<b>0.275</b>	0.212	0.320
	336	<b>0.197</b>	<b>0.304</b>	0.238	0.343
	720	<b>0.248</b>	<b>0.347</b>	0.309	0.400
Exchange	96	<b>0.109</b>	<b>0.232</b>	0.112	0.238
	192	0.280	0.375	<b>0.265</b>	<b>0.371</b>
	336	<b>0.472</b>	0.504	0.501	<b>0.502</b>
	720	<b>1.241</b>	<b>0.823</b>	1.610	0.942
TrafficL	96	<b>0.405</b>	<b>0.286</b>	0.468	0.332
	192	<b>0.421</b>	<b>0.297</b>	0.490	0.347
	336	<b>0.448</b>	<b>0.318</b>	0.531	0.371
	720	<b>0.527</b>	<b>0.362</b>	0.602	0.400
Weather	96	<b>0.164</b>	<b>0.199</b>	0.167	0.200
	192	<b>0.224</b>	<b>0.255</b>	0.226	0.255
	336	0.285	0.311	<b>0.284</b>	<b>0.297</b>
	720	0.366	0.359	<b>0.360</b>	<b>0.352</b>
P. Diff.	96	<b>-8.911</b>	<b>-6.251</b>	0.000	0.000
	192	<b>-7.544</b>	<b>-6.085</b>	0.000	0.000
	336	<b>-8.740</b>	<b>-4.575</b>	0.000	0.000
	720	<b>-15.22</b>	<b>-8.318</b>	0.000	0.000

**Table A4.** Empirical evaluation of long multi-horizon multivariate forecasts for N-HiTS with different hierarchical orders. All other hyperparameters were kept constant across all datasets. MAE and MSE for predictions averaged over eight seeds, the best result is highlighted in bold (lower is better). Average percentage difference relative to ascending hierarchy in the last panel.

		Top-Down		Bottom-Up	
		MSE	MAE	MSE	MAE
ETTm2	96	<b>0.185</b>	<b>0.265</b>	0.191	0.266
	192	<b>0.244</b>	<b>0.308</b>	0.261	0.320
	336	<b>0.301</b>	<b>0.347</b>	0.302	0.353
	720	<b>0.429</b>	<b>0.438</b>	0.440	0.454
ECL	96	<b>0.152</b>	<b>0.257</b>	0.164	0.270
	192	<b>0.172</b>	<b>0.275</b>	0.186	0.292
	336	<b>0.197</b>	<b>0.304</b>	0.217	0.327
	720	<b>0.248</b>	<b>0.347</b>	0.273	0.369
Exchange	96	<b>0.109</b>	<b>0.232</b>	0.114	0.242
	192	<b>0.280</b>	<b>0.375</b>	0.436	0.452
	336	<b>0.472</b>	<b>0.504</b>	0.654	0.574
	720	<b>1.241</b>	<b>0.823</b>	1.312	0.861
TrafficL	96	<b>0.405</b>	<b>0.286</b>	0.410	0.292
	192	<b>0.421</b>	<b>0.297</b>	0.427	0.305
	336	<b>0.448</b>	<b>0.318</b>	0.456	0.323
	720	<b>0.527</b>	<b>0.362</b>	0.557	0.379
Weather	96	0.164	<b>0.199</b>	<b>0.163</b>	0.200
	192	0.224	0.255	<b>0.219</b>	<b>0.252</b>
	336	<b>0.285</b>	0.311	0.288	0.311
	720	0.366	0.359	<b>0.365</b>	<b>0.355</b>
P. Diff.	96	<b>-2.523</b>	<b>-2.497</b>	0.000	0.000
	192	<b>-12.296</b>	<b>-6.793</b>	0.000	0.000
	336	<b>-11.176</b>	<b>-5.507</b>	0.000	0.000
	720	<b>-4.638</b>	<b>-3.699</b>	0.000	0.000

#### A.4.3. ORDER OF HIERARCHICAL REPRESENTATIONS

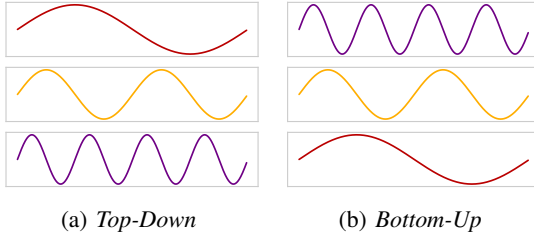


Figure 4. Hierarchical representation configurations.

Deep Learning in classic tasks like computer vision and natural language processing is known to learn hierarchical representations from raw data that increase complexity as the information flows through the network. This automatic feature extraction phenomenon is believed to drive to a large degree the algorithms' success (Bengio et al., 2012).

Our approach differs from the conventions in the sense that we use a *Top-Down* hierarchy where we prioritize in the synthesis of the predictions to low frequencies and sequentially complement them with higher frequencies details, as explained in Section 3. We achieve this with N-HiTS' *expressiveness ratio* schedules.

Our intuition is that the *Top-Down* hierarchy acts as a regularizer and helps the model to focus on the broader factors driving the predictions rather than narrowing its focus at the beginning on the details that compose them. To test these intuitions, we designed an experiment where we inverted the expressiveness ratio schedule into *Bottom-Up* hierarchy predictions and compared the validation performance.

Remarkably, as shown in Table A4, the *Top-Down* predictions consistently outperform the *Bottom-Up* counterpart. Relative improvements in MAE are 4.6%, in MSE of 7.5%, across horizons and datasets.

Our observations match the forecasting community practice that addresses long-horizon predictions by first modeling the long-term seasonal components and then its residuals. Research on long-horizon forecasting has primarily focused on long-term seasonal component, as it is a common belief that it is the most important.

## A.5. Hyperparameter Optimization Resources

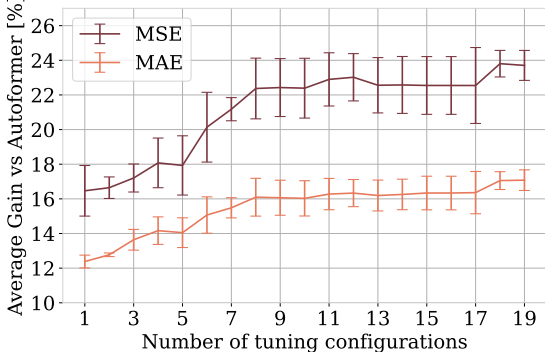


Figure 5. N-HiTS performance improvement over Autoformer as a function of explored hyperparameter configurations.

Computational efficiency has important implications for the prediction’s accuracy and the cost of deployment of the algorithms. In particular, because forecasting systems are constantly retrained to address distributional shifts, orders-of-magnitude improvements in speed can easily translate into orders-of-magnitude price differences deploying the models. This section explores the implications of computational efficiency in the accuracy gains associated with hyperparameter optimization and training economic costs.

**Hyperparameter Optimization.** Despite all the progress improving the computation efficiency of Transformer-based methods, see Figure 5, their speed and memory requirements make exploring their hyperparameter space unaffordable in practice, considering the amount of GPU computation they still require. The diminishing returns nature of the exploration gains makes this problem even more pronounced.

For this experiment we report the iterations of the *hyperparameter optimization phase*, described in Section 4.4, where we explore the hyperparameters from Table 3 using HYPEROPT, a Bayesian hyperparameter optimization library (Bergstra et al., 2011). As shown in Figure 5 the exploration exhibits monotonic relative performance gains of N-HiTS versus the best reported Autoformer (Wu et al., 2021) in the ablation datasets.

**Training Economic Costs.** We measure the train time for N-HiTS, N-BEATS<sub>G</sub> and Transformer-based models, on the six main experiment datasets and 8 runs. We rely on a AWS g4dn.2xlarge, with an NVIDIA T4 16GB GPU.

We differentiate between N-HiTS<sub>1</sub>, our method with a single HYPEROPT iteration randomly sampled from Table 3, and N-HiTS<sub>20</sub> to our method after 20 HYPEROPT iterations. For the Transformer-based models we used optimal hyperparameters as reported in their repositories.

Table A5 shows the measured train time for the models, N-HiTS<sub>1</sub> takes 1.5 hours while more expensive architectures like Autoformer or Informer take 92.6 and 62.1 hours each. Based on hourly prices from January 2022 for the g4dn.2xlarge instance, USD 0.75, the main results of the paper would cost nearly USD 70.0 with Autoformer, USD 46.5 with Informer, while N-HiTS<sub>1</sub> results can be executed under USD 1.5 and N-HiTS<sub>20</sub> with USD 22.8. Figure 5, shows that N-HiTS<sub>1</sub> achieves a 17% MSE average performance gain over Autoformer with 1.6% of a single run cost, and N-HiTS<sub>20</sub> almost 25% gain with 33% of a single run cost. A single run does not consider hyperparameter optimization.

$$\text{ExptPrice} = \text{GPUPrice} \times \text{HyperOptIters} \times \text{TrainTime} \times \text{Runs}$$

Table A5. Train time in hours for N-HiTS and Transformer-based architectures on a g4dn.2xlarge instance.

Horizon	N-HiTS <sub>1</sub>	N-HiTS <sub>20</sub>	Autoformer	Informer	N-BEATS <sub>G</sub>
A. Time					
96/24	0.183	3.66	12.156	9.11	0.291
192/36	0.257	5.14	16.734	11.598	0.462
336/48	0.398	7.96	22.73	15.237	0.674
720/60	0.682	13.64	40.987	26.173	1.249
Total	1.523	30.46	92.607	62.118	2.676

## A.6. Univariate Forecasting

As a complement of the main results from Section 4.3, in this Appendix, we performed univariate forecasting experiments for the ETT<sub>m2</sub> and Exchange datasets. This experiment allows us to compare closely with other methods specialized in long-horizon forecasting that also considered this setting (Zhou et al., 2020; Wu et al., 2021).

For the univariate setting, we consider the Transformer-based (1) Autoformer (Wu et al., 2021), (2) Informer (Zhou et al., 2020), (3) LogTrans (Li et al., 2019) and (4) Reformer (Kitaev et al., 2020) models. We selected other well-established univariate forecasting benchmarks: (5) N-BEATS (Oreshkin et al., 2020), (6) DeepAR (Salinas et al., 2020) model, which takes autoregressive features and combines them with classic recurrent networks. (7) Prophet (Taylor & Letham, 2018), an additive regression model that accounts for different frequencies non-linear trends, seasonal and holiday effects and (8) an auto ARIMA (Hyndman & Khandakar, 2008).

**Forecasting Accuracy.** Table A6 summarizes the univariate forecasting results. N-HiTS significantly improves over the alternatives, decreasing 17% in MAE and 25% in MSE across datasets and horizons, with respect the best alternative. As noticed by the community recurrent based strategies like the one from ARIMA, tend to degrade due to the concatenation of errors phenomenon.

*Table A6.* Empirical evaluation of long multi-horizon **univariate** forecasts. *Mean Absolute Error* (MAE) and *Mean Squared Error* (MSE) for predictions averaged over eight runs, the best result is highlighted in bold (lower is better). We gradually prolong the forecast horizon.

\* The automatic ARIMA model has a unique solution, for which its results do not have variance. The evident long-horizon degradation of its performance follows from compounding prediction errors.

		N-HiTS		Autoformer		Informer		LogTrans		Reformer		N-BEATS		DeepAR		Prophet		ARIMA <sup>*</sup>	
		MSE	MAE	MSE	MAE	MSE	MAE	MSE	MAE	MSE	MAE	MSE	MAE	MSE	MAE	MSE	MAE	MSE	MAE
ETTm2	96	0.066	<b>0.185</b>	<b>0.065</b>	0.189	0.088	0.225	0.082	0.217	0.131	0.288	0.082	0.219	0.099	0.237	0.287	0.456	0.211	0.362
	192	<b>0.087</b>	<b>0.223</b>	0.118	0.256	0.132	0.283	0.133	0.284	0.186	0.354	0.120	0.268	0.154	0.310	0.483	0.261	0.406	
	336	<b>0.106</b>	<b>0.251</b>	0.154	0.305	0.180	0.336	0.201	0.361	0.220	0.381	0.226	0.370	0.277	0.428	0.331	0.474	0.317	0.448
Exchange	720	<b>0.157</b>	<b>0.312</b>	0.182	0.335	0.300	0.435	0.268	0.407	0.267	0.430	0.188	0.338	0.332	0.468	0.534	0.593	0.366	0.487
	96	<b>0.093</b>	<b>0.223</b>	0.241	0.299	0.591	0.615	0.279	0.441	1.327	0.944	0.156	0.299	0.417	0.515	0.828	0.762	0.112	0.245
	192	<b>0.230</b>	<b>0.313</b>	0.273	0.665	1.183	0.912	1.950	1.048	1.258	0.924	0.669	0.665	0.813	0.735	0.909	0.974	0.304	0.404
	336	<b>0.370</b>	<b>0.486</b>	0.508	0.605	1.367	0.984	2.438	1.262	2.179	1.296	0.611	0.605	1.331	0.962	1.304	0.988	0.736	0.598
	720	<b>0.728</b>	<b>0.569</b>	0.991	0.860	1.872	1.072	2.010	1.247	1.280	0.953	1.111	0.860	1.890	1.181	3.238	1.566	1.871	0.935